Structural Engineering and Mechanics, *Vol. 49, No. 3 (2014) 329-353*
DOI: http://dx.doi.org/10.12989/sem.2014.49.3.329

Design of LQR controller for active suspension system of Partially Filled Tank Cars

Mohammad Mahdi Feizi* and Mohammad Ali Rezvani[a]

School of Railway Engineering, Iran University of Science and Technology, Narmak, Tehran 16745-1833, Iran

(Received July 22, 2012, Revised December 24, 2013, Accepted December 27, 2013)

Abstract. Increasing usage of tank cars and their intrinsic instability due to sloshing of contents have caused growing maintenance costs as well as more frequent hazards and defects like derailment and fatigue of bogies and axels. Therefore, varieties of passive solutions have been represented to improve dynamical parameters. In this task, assuming 22 degrees of freedom, dynamic analysis of partially filled tank car traveling on a curved track is investigated. In order to consider stochastic geometry of track; irregularities have been derived randomly by Mont Carlo method. More over the fluid tank model with 1 degree of freedom is also presented by equivalent mechanical approach in terms of pendulum. An active suspension system for described car is designed by using linear quadratic optimal control theory to decrease destructive effects of fluid sloshing. Eventually, the performance of the active suspension system has been compared with that of the passive one and a study is carried out on how active suspension may affect the dynamical parameters such as displacements and Nadal's derailment index.

Keywords: tank cars; sloshing; fluid solid interaction; dynamic stability; derailment; active suspension system

1. Introduction

Parallel to the widespread use of the tank cars, the need for increasing the capacity and maneuverability of these cars has been highlighted. Tank cars carry variety of liquids and naturally endure liquid sloshing during travel especially at curves. For the rail vehicles traveling at curves the derailment quotient and unloading ratio that represent the dynamic stability of the rolling stock are 18% and 25% different compared to the cases without sloshing (Younesian 2010). In addition to lateral instability, the liquid sloshing can cause longitudinal instability during the vehicle deceleration (braking) and acceleration. Logically, instability in motion deteriorates the wheel/rail contact conditions and subsequently increases the wheel/rail wear. The undesirable effects of sloshing causing fatigue in the vehicle structure and in the elements of its suspension system need further attention. Fatigue is related to the harmonic motion within the liquid (Prabhakaran 2005) that is caused by the sloshing. Fatigue in the axle of a tank car has been analyzed by using the

∗Corresponding author, Research Student, E-mail: mm_feizi@rail.iust.ac.ir
[a]Assistant Professor, E-mail: rezvani_ma@iust.ac.ir

http://www.techno-press.org/?journal=sem&subpage=8 ISSN: 1225-4568 (Print), 1598-6217 (Online)

Fig. 1 Fracture at axle mounting point in a tank car caused by the fatigue and derailment (Locovei 2010)

finite elements method (Locovei 2010). An axle enduring fatigue can easily fail under sever excitation such as the derailment forces. A failed axle after derailment is presented in Fig. 1, (Locovei 2010). In order to control the liquid movements it was a common practice to use specially designed internal equipments and baffles in tank cars. However, it was suggested that such equipment can cause damages to the tank shells especially at low ambient temperatures. The use of such equipments is not recommended (GM/GN 2010). However, this further highlights the need for noticing the liquid sloshing and providing safety in transportation.

It is a common practice to use the finite element method and the equivalent dynamic method for the simulation of the sloshing caused by different mechanical forces. Ormeño *et al*. (2012) have investigated the influence of uplift on liquid storage tanks during earthquakes and six ground motions tested by scaled shake table. For FEM modeling and the continuous solution, the different types of vessels such as cylindrical, rectangular and other shapes were analyzed experimentally and numerically. In these studies the interaction of solid and fluid and associated parameters like pressure using arbitrary Lagrange Euler and similar methods were simulated. Cakir *et al.* (2013), developed the non-linear three dimensional (3D) finite element models using numerical and experimental investigations performed on the backfill- exterior wall-fluid interaction systems in case of empty and full tanks. Research in this field proves that the predictions for the forces generated by the liquid sloshing in these two methods are reasonably compatible (Ali abadi 2003). Suarez *et al*. (2005) worked on the dynamic simulation of tank cars by using the equivalent dynamic method. They used the equivalent mass-spring dynamic model for the analysis. The tank was considered as a rectangular cube. Four cars were coupled and studied during the braking and acceleration processes. Responses in the couplers were used for further processing. The analyses were numerical and SIMPACK engineering software was used (Vera 2005). Younesian *et al*. (2010) studied the dynamic behavior of the tank car at cures by using the equivalent dynamic (mass-spring) model. They used ADAMAS/RAIL engineering software for the multi-body simulation and analysis of the subject (Younesian 2010). There are also many studies that are based on the analytical methods and are concerned with the dynamic analysis of rail car. Wang (1992) used a model containing 23 degrees of freedom, including 5 for the car body and 3 for the bolster. The study of the rolling stock at curve through a nonlinear solution method including 8 and 10 degrees of freedom for the vehicle was reported by Lee *et al.* (2005, 2006). Zeng and Wu (2004) used a model with 17 degrees of freedom in it. Cheng *et al.* (2009) studied the nonlinear stability (hunting) in high speed trains at curves by using a model with 21 degrees of freedom. They used a non linear Heuristic model to extract the spin creep forces.

Nowadays it is a common practice in the railway rolling stocks to use active suspension in order to increase the passenger comfort and to provide dynamic stability for high speed trains

(Zhou 2011). However, due to the mechanical difficulties this is not practiced for freight wagons.

There is no end for the increasing demand for the freight wagons. The tank cars are also one the most important part of the fleet. They carry liquids and while in travel they encounter sloshing. Subsequently tank cars endure sloshing forces that can inflict damage on the tank shells and shorten their service life. This can build up huge cost for maintaining the system. Bearing these in mind has urged the need for this research that proposes the inclusion of the active suspension systems in tank cars.

Practically, there is no readymade analytical method that is concerned with the solution of the motion equations for the tank cars. The common practices in such cases are resorting to the numerical methods and simulation by using the available engineering software.

This research proposes a model for the tank car that includes 22 degrees of freedom. The analysis is concerned with the dynamic behavior of a tank car equipped with Y25 bogies traveling at curve. Amongst the 22 degrees of freedom, 21 correspond to the vehicle and 1 corresponds to the lateral motion of the liquid. Wheelsets are assumed to have the yaw and the lateral motions. The wheel/rail contact is provided with the assumption of linear creepage. Four degrees of freedom correspond to each bogie including the lateral and the vertical displacements, the yaw and the roll motions. Five degrees of freedom correspond to the Car body including the vertical and the longitudinal displacements, the yaw, roll and pitch motions. Sloshing in the liquid is modeled by using the equivalent mechanical model that represents a pendulum. The proposal includes the design of an active suspension system of LQR type. This is aimed at improving the curving behavior of the tank car and reducing the damages to the tank car equipment. The dynamic behavior of the tank car with the inclusion of the active suspension system is investigated. The results are compared for the tank cars with and without the proposed suspension system. The variation in the Nadal's derailment index is also investigated.

2. The Modeling procedure

2.1 The vehicle

The national railway of France (SNCF) started studies in order to improve its' freight fleet in the 60^{th}. Part of the job was to design a bogie with lower volume and mass compared to the existing bogies of the time. They ended up introducing the Y25 bogies with the axle distance of 2 meters and the wheel diameter of 920 mm. The design included coil springs in the primary suspension instead of the leaf springs. This was satisfactory up to some extent. After rewriting the standards for the freight bogies in 1966, the Y25 bogies with the axle distance of 1800 mm were designed and manufactured.

This research for its modeling purposes uses the structural data for a tank car that is manufactured locally by Wagon Pars limited. The tank on this car has a volume of 65 m^3 and is equipped with two Y25 bogies. The Schematic side view of the tank car is presented in Fig. 5.

2.2 Friction pads and the equivalent viscous dampers

Presence of the friction forces makes the numerical modeling of the freight bogies a tedious task. Generally, in such cases the system motion equations are nonlinear. In order to resolve the problem, it is a common practice to replace the friction pads with viscous dampers in the modeling

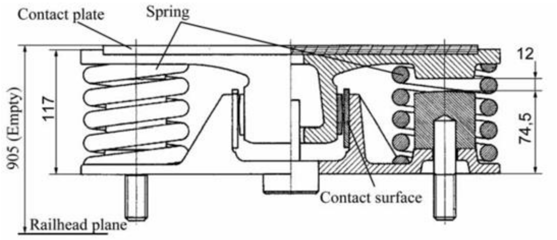

Fig. 2 The side bearer in Y25 Bogie (Evans 1998)

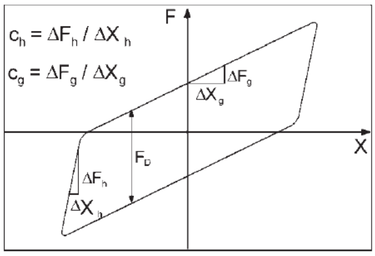

Fig. 3(a) The hysteresis (force-displacement) diagram for the Y25 friction pads

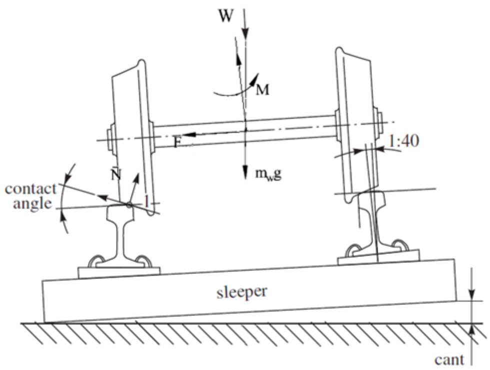

Fig. 3(b) Free body diagram of wheelset

Table 1 Measured data for the Y25 bogie suspension system (Molatefi 2006)

	x			*y*			*z*	
C_h (N/m)	C_g (N/m)	F_D (kN)	C_h (N/m)	C_g (N/m)	F_D (kN)	C_h (N/m)	C_g (N/m)	F_D (kN)
1.3×10^7	8.9×10^5	2.5	2.2×10^6	4.3×10^5	5.0	1.7×10^7	8.5×10^5	4.0

procedure. Tan *et al*. (1995) exercised the idea of the equivalent viscous damping to replace the coulomb friction while studying vibrating systems with multi degrees of freedom. Such idealization provides the proper conditions for the design of a controller for the liquid sloshing. In Y25 bogies there are the contact surfaces that are known as the side bearers and in planar motion tolerate friction forces. To serve the purpose, they are replaced with the equivalent viscous dampers through the method described, hereunder. The schematic of the side bearer in Y25 bogie is presented in Fig. 2. The corresponding force-displacement diagram is presented in Fig. 3 (a) and (b).

Further measured data for these side bearers are presented in Table 1, (Molatefi 2006). By calculating the area under the hysteresis curve the damped energy (*W*) and subsequently the equivalent viscous damping (*C*) can be calculated.

2.3 The wheelset motion equations

By considering the horizontal and the yaw degrees of freedom the linear creep model is used in order to model the wheel/rail contact forces. By equating the saturation index α with 1 the wheelset motion equations presented by Cheng (2009), transform from nonlinear to a linear set. Such method is useful and accurate especially for the dynamic analysis of the vehicle at curves with large radius. In the following equations *i*=1, 2 represent the rear and the front bogies, *j*=1, 2 represent the rear and the front wheel, *k*=1,2 represent the control forces at the left and the right sides of the bogie. *V* represents the fleet speed of travel at the curve of radius R and the inclination cant angle of ϕ_{se}.

$$m_w\left(\ddot{y}_{wij}-\frac{V^2}{R}\right)=\frac{2f_{11}}{V}\left(\dot{y}_{wij}-V\psi_{wij}\right)-\frac{2f_{12}}{V}\left(\dot{\psi}_{wij}-\frac{V}{R}\right)-\frac{2r_0f_{11}}{V}\left(\frac{\lambda}{a}\right)\dot{y}_{wij}-\left(W_{ext}+m_wg+\frac{V^2W_{ext}}{gR}\phi_{se}\right)\left(\frac{\lambda}{a}\right)y_{wij}-(W_{ext}+m_wg)\phi_{se}+\frac{V^2W_{ext}}{gR}+F_{syij} \quad (1)$$

$$I_{wz}\ddot{\psi}_{wij}=-\frac{2a\lambda f_{33}}{r_0}y_{wij}+\frac{2f_{12}}{V}\dot{y}_{wij}-\left(I_{wy}\frac{V}{r_0}-\frac{2r_0f_{12}}{V}\right)\left(\frac{\lambda}{a}\right)y_{wij}-2f_{12}\psi_{wij}+\left(W_{ext}+m_wg+\frac{V^2W_{ext}}{gR}\phi_{se}\right)a\lambda\psi_{wij}+M_{szij}-\left(\frac{2a^2f_{33}}{V}+\frac{2f_{22}}{V}\right)\dot{\psi}_{wij}+\frac{2}{R}(a^2f_{33}+f_{22}) \quad (2)$$

$$\delta_L=\delta_R=\lambda,\quad \tfrac{1}{2}(r_L-r_R)=\lambda y_{wij},\ \tfrac{1}{2}(r_L-r_R)=r_0 \quad (3)$$

In this modeling it is assumed that in curving there is no contact between the wheel flange and the rail. It means that during curving the train is in static equilibrium and the vertical forces remain constant, regardless of the track irregularities (Cheng 2009). For the same reason, the train wheelset model is based on the equivalent conical wheels. With this purpose in mind, conicity of the left and the right wheels are set equal to λ.

$$F_{syij}=-2K_{py}y_{wij}-(-1)^j2K_{py}L_1\psi_{ti}+2K_{py}y_{ti}-2C_{py}\dot{y}_{wij}-(-1)^j2C_{py}L_2\dot{\psi}_{ti}+2C_{py}\dot{y}_{ti}+2K_{py}h_T\phi_{ti}+2C_{py}h_T\dot{\phi}_{ti} \quad (4)$$

$$M_{szij}=2K_{px}b_1^2\psi_{ti}+2C_{px}b_1^2\dot{\psi}_{ti}-2K_{px}b_1^2\psi_{wij}-2C_{px}b_1^2\dot{\psi}_{wij} \quad (5)$$

With the assumption of the static equilibrium in the rolling stock, the vertical forces acting on the wheelset at curves are calculated according to Eq. (6). It needs to be emphasized that the Kalker's creep coefficients (that are used for the modeling of the contact forces) vary by the variations in the vertical forces between the wheel and the rail and also by variations in the wheel profile. Therefore, with the assumption of modeling the conical wheels under the stable static conditions theses coefficients remain constant

$$N^n_{Lyij}=N^n_{Rzij}=\tfrac{1}{2}\left(W_{ext}+m_wg+\frac{V^2W_{ext}}{gR}\phi_{se}\right) \quad (6)$$

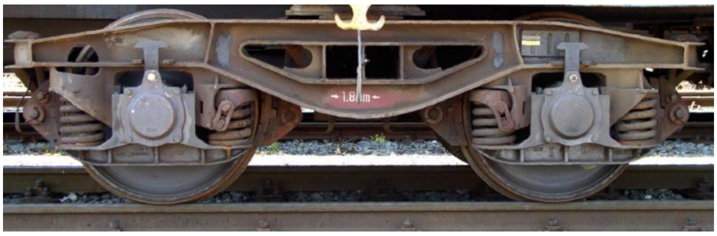

Fig. 4 Side view of Y25 bogie

2.4 The bogie motion equations

The bogie models include 4 degrees of freedom for each bogie. Two of the freedoms correspond to the displacements in the in lateral (*y*) and vertical (*z*) directions and two correspond to the roll and the yaw motions. The equivalent viscous dampers are used instead of the friction dampers. A picture presenting the side view of the Y25 bogie is presented in Fig. 4.

$$m_t\ddot{y}_{ti} = F_{syti} + \left(\frac{V^2}{gR} - \phi_{se}\right)m_t \tag{7}$$

$$m_t\ddot{z}_{ti} = F_{szti} + \left(1 + \frac{V^2}{gR}\phi_{se}\right)m_t g \tag{8}$$

$$I_{tx}\ddot{\phi}_{ti} = M_{sxti} \tag{9}$$

$$I_{tz}\ddot{\psi}_{ti} = M_{szti} \tag{10}$$

$$\begin{gathered} F_{syti} = -2K_{py}y_{wij} + 2C_{px}\dot{y}_{wij} + \left(-4K_{py} - 2K_{Sy}\right)y_{ti} + \left(4C_{py} - 2C_{sy}\right)\dot{y}_{ti} + 2K_{sy}L_c\psi_c \\ +2C_{sy}L_c\dot{\psi}_c + 2K_{sy}y_c + 2C_{sy}\dot{y}_c + 2K_{sy}(h_c - h_T)\phi_c + 2C_{sy}(h_c - h_T)\dot{\phi}_c - 4K_{py}h_T\phi_{ti} \\ -4C_{py}h_T\dot{\phi}_{ti} \end{gathered} \tag{11}$$

$$F_{szti} = 2K_{sz}z_c + 2C_{sz}\dot{z}_c - 2\left(K_{sz} + 2K_{pz}\right)z_{ti} - 2\left(C_{sz} + 2C_{pz}\right)\dot{z}_{ti} + \sum_{k=1}^{2}(-1)^{k+1}F_{ik} \tag{12}$$

$$2K_{py}h_T^2\phi_{ti} - 4C_{py}h_T^2\dot{\phi}_{ti} - 4K_{pz}b_1^2\phi_{ti} - 4C_{pz}b_1^2\dot{\phi}_{ti} + \sum_{k=1}^{2}(-1)^{k+1}F_{ik}b_2 \tag{13}$$

$$\begin{gathered} M_{szti} = \left(-4K_{py}L_1^2 - 4K_{px}b_1^2 - 2K_{sx}b_2^2\right)\psi_{ti} + \left(-4C_{py}L_2^2 - 4C_{px}b_1^2 - 2C_{sx}b_3^2\right)\dot{\psi}_{ti} \\ +2K_{py}L_1y_{wi1} + 2C_{py}L_2\dot{y}_{wiL} + 2K_{px}b_1^2\psi_{wi1} + 2C_{px}b_1^2\dot{\psi}_{wi1} - 2K_{py}L_1y_{wi2} - 2C_{py}L_2\dot{y}_{wiL} \\ +2K_{px}b_1^2\psi_{wi2} + 2C_{px}b_1^2\dot{\psi}_{wi2} + 2K_{sx}b_2^2\psi_c + 2C_{sx}b_3^2\dot{\psi}_c \end{gathered} \tag{14}$$

2.5 The car body motion equations

In the modeling of the tank car the degrees of freedom include the lateral *y*, and the vertical *z* displacements and the yaw, the roll and the pitch motions for the car body. The schematic of the tank car is presented in Fig. 5. The motion equations associated with the car body degrees of freedom are presented in the Eqs. (15) to (24)

$$m_c\ddot{y}_c = F_{syc} + \left(\frac{V^2}{gR} - \phi_{se}\right)m_c g \tag{15}$$

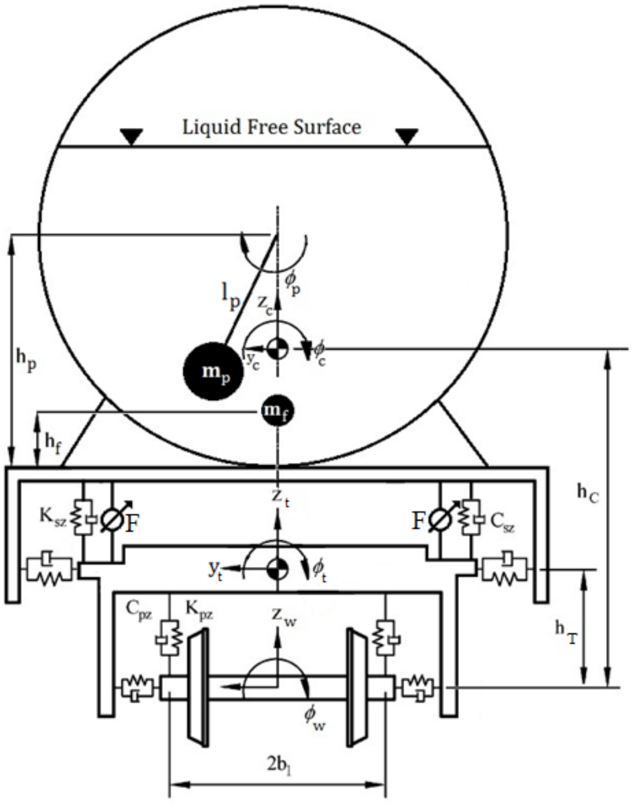

Fig. 5 Idealization of the tank car representing its degrees of freedom

$$m_c\ddot{z}_c = F_{szc} + \left(1 + \frac{V^2}{gR}\phi_{se}\right) m_c g \tag{16}$$

$$I_{cx}\ddot{\phi}_c = M_{sxc} \tag{17}$$

$$I_{cy}\ddot{\theta}_c = M_{syc} \tag{18}$$

$$I_{cz}\ddot{\psi}_c = M_{szc} \tag{19}$$

$$\begin{aligned} F_{syc} = &-2K_{sy}(2y_c - y_{t1} - y_{t2}) - 4K_{sy}(h_c - h_T)\phi_c - 2C_{sy}(2\dot{y}_c - \dot{y}_{t1} - \dot{y}_{t2}) \\ &-4C_{sy}(h_c - h_T)\dot{\phi}_c + m_p\, l_p\ddot{\phi}_p \end{aligned} \tag{20}$$

$$F_{szc} = -4K_{sz}z_c - 4C_{sz}\dot{z}_c + 2K_{sz}z_{t1} + 2C_{sz}\dot{z}_{t1} + 2K_{sz}z_{t2} + 2C_{sz}\dot{z}_{t2} + \sum_{i=1}^{2}\sum_{k=1}^{2}(-1)^{k+1}F_{ik} \tag{21}$$

$$\begin{aligned} M_{sxc} = &\,2K_{sz}b_2^2\phi_{t1} + 2C_{sz}b_3^2\dot{\phi}_{t1} + 2K_{sz}b_2^2\phi_{t2} + 2C_{sz}b_3^2\dot{\phi}_{t2} - 4K_{sz}b_2^2\phi_c - 2C_{sz}b_3^2\dot{\phi}_c \\ &-4K_{sy}(h_c - h_T)y_c - 4C_{sy}(h_c - h_T)\dot{y}_c + 2K_{sy}(h_c - h_T)y_{t1} + 2C_{sy}(h_c - h_T)\dot{y}_{t1} \\ &+2K_{sy}(h_c - h_T)y_{t2} + 2C_{sy}(h_c - h_T)\dot{y}_{t2} - 4K_{sy}(h_c - h_T)^2\phi_c - 4C_{sy}(h_c - h_T)^2\dot{\phi}_c \\ &-4K_{sy}(h_c - h_T)L_c\psi_c - 4C_{sy}(h_c - h_T)L_c\dot{\psi}_c + m_p\, l_p h\ddot{\phi}_p + \sum_{i=1}^{2}\sum_{k=1}^{2}(-1)^k F_{ik}b_2 \end{aligned} \tag{22}$$

$$M_{syc} = -2K_{sz}z_{t1} + 2K_{sz}z_{t2} - 4K_{sz}\theta_c L_c - 2C_{sz}\dot{z}_{t1} + 2C_{sz}\dot{z}_{t2} \\ -4C_{sz}\dot{\theta}_c L_c + \sum_{i=1}^{2}\sum_{k=1}^{2} (-1)^{k+1} F_{ik} l_c \tag{23}$$

$$M_{szc} = -4K_{sy}\psi_c L_c^2 - 4C_{sy}\dot{\psi}_c L_c^2 - 2K_{sx}b_2^2(2\psi_c - \psi_{t1} - \psi_{t2}) - 2C_{sx}b_3^2\left(2\dot{\psi}_c - \dot{\psi}_{t1} - \dot{\psi}_{t2}\right) \\ -2K_{sy}L_c(-y_{t1} - y_{t2}) - 2C_{sy}L_c(-\dot{y}_{t1} - \dot{y}_{t2}) \tag{24}$$

2.6 Modeling the liquid sloshing

2.6.1 Mechanical simulation of sloshing

Two common methods for the modeling of the liquid sloshing include the mass-spring and the pendulum models. The past experiences prove that for tanks with circular shells under lateral excitations the pendulum model provides more accurate results for liquid sloshing (Sumner 1965). The modeling involves dividing the liquid into two segments with one segment in motion and the other segment stagnant. The moving segment is modeled as a pendulum while the stagnant segment is modeled as a stationary mass. Particulates of the pendulum, the stationary mass and their locations are presented in Fig. 6 (Abramson 1966). While the vibration of the car and fluid sloshing interact with each other, the 1st mode of vibration of fluid sloshing is the dominant mode in exciting the tank car; therefore it is used for further calculations. In Fig. 6 h is the height of the liquid measured from the bottom of the tank, *R* is the radius of the tank, *lp* is the length of the pendulum, m is the total mass of the liquid, *mp* is the mass of the pendulum and *ho* is the height of the stagnant mass measured from the bottom of the tank. The stationary mass mf is the difference between the total mass and the equivalent mass of the pendulum. For the purposes of the modeling of maximum free surface of fluid, it is assumed that the tank is half full. Under such condition the liquid has the maximum free space to move around inside the tank.

2.6.2 Liquid sloshing equations

As mentioned before, the liquid sloshing during the train maneuvers at curves is modeled by a pendulum with on degree of freedom (Fig. 5). The number of fluid sloshing modes determines the degree of freedom and number of pendulums finally. The liquid motions in all other directions are

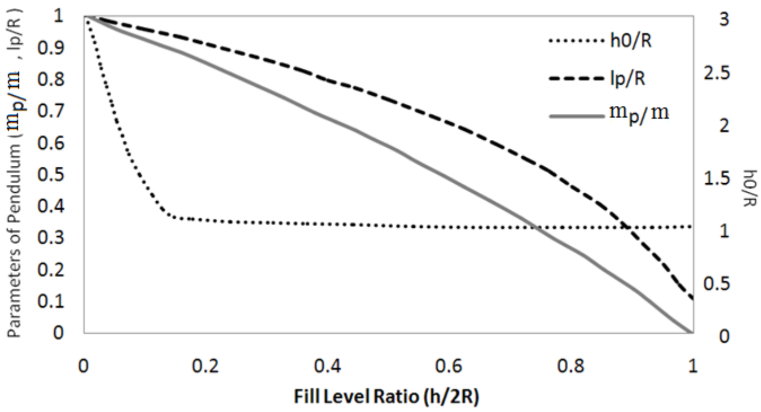

Fig. 6 Specifications of the pendulum model needed for the modeling of liquid sloshing (Abramson 1966)

ignored. In Eq. (25) ϕ_p represents the pendulum degree of freedom and is the rotation around the *x* axis where the pendulum connects to the car. *hi* is the distance between the body centroid and the mass centroid of the car. In the derivation of the following equation it is assumed that the pendulum rotates at small angles.

$$I_p\ddot{\phi}_p + m_p g l_p \phi_p + m_p h_i l_p \ddot{\phi}_c + m_p \ddot{y}_c l_p = 0 \tag{25}$$

2.6.2 1 Transformation of the sloshing equation form to common forms

In order to calculate equivalent mass, stiffness and damping matrices of system, the $\ddot{y}_c$ and $\ddot{\phi}_c$ are obtained from Eq. (15) and Eq. (17) and substituted for in Eq. (25). With these substitutions interest matrices are easily calculated.

3. Solving the set of motion equations

3.1 The initial conditions

3.1.1 The track irregularities

Considering the random nature of the track irregularities, the power spectral density (PSD) functions are used to represent them (Frýba 1996). The track irregularity classifications are defined by the Federal Railroad Administration (FRA), USA. They are categorized into 6 classes ranging from 1 to 6 representing tracks with the highest and the lowest irregularities. Eqs. (26) and (27) represent PSD functions that are defined by FRA including *Sc,g* cross and gauge and *Se,a* elevation and alignment (Wiriyachai 1982).

$$S_{c,g}(\Omega) = \frac{A\Omega_2^2}{(\Omega^2+\Omega_1^2)(\Omega^2+\Omega_2^2)} \tag{26}$$

$$S_{e,a}(\Omega) = \frac{A\Omega_2^2(\Omega^2+\Omega_1^2)}{\Omega^4(\Omega^2+\Omega_2^2)} \tag{27}$$

Where $S(\Omega)$ is the PSD for the track irregularities in wavelength. $\Omega = (\frac{2\pi}{v\times\omega})$ where v is the car speed of travel. $A(m3)$, Ω1 and Ω2 are constants that depend on the rail classification and are given for the class 3 of rails in Table 2.

Table 2 The track irregularity related coefficients for rail class 3 (Frýba 1996)

Irregularity	Parameter		Track class
	Notation	Unit	3
Elevation	A	10^8 m^3	4.92
	Ω_1	10^3 m^{-1}	23.3
	Ω_2	10^3 m^{-1}	13.1
Gauge	A	10^8 m^3	3.15
	Ω_1	10^3 m^{-1}	29.2
	Ω_2	10^3 m^{-1}	23.3

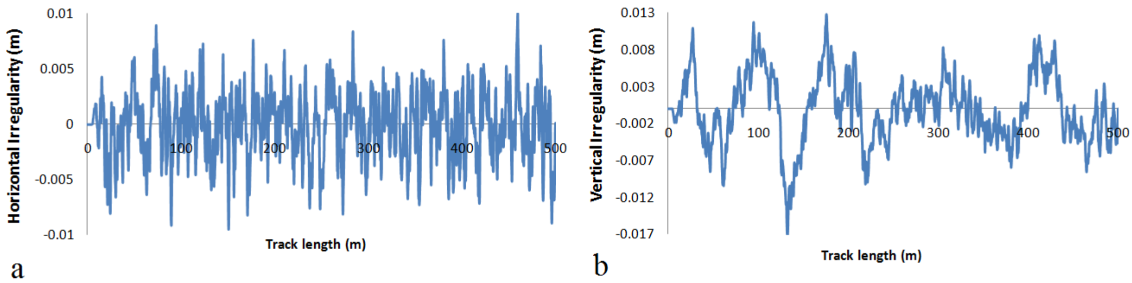

Fig. 7 (a) Grade 3 of the track horizontal irregularities (b) Grade 3 of the track vertical irregularities, reproduced by using data from Frýba (1996)

The method proposed by Au *et al.* (2002) that is given in Eq. (28) is used in order to calculate the track irregularity versus location $r(x)$.

$$r(x) = \sum_{k=1}^{N} a_k \cos(\omega_k x + \varphi_k) \tag{28}$$

In this equation a_k is the amplitude, ω_k is the frequency domain $[\omega_1, \omega_2]$ in which the calculations are performed and φ_k is a random number in the normal domain of $[0, 2\pi]$. Also x represents the location on the track and N is the number of divisions in the domain. a_k and ω_k are calculated according to the Eqs. (29) and (30)

$$a_k = 2\sqrt{S(\omega_k)\Delta\omega} \qquad k = 1,2,\dots,N \tag{29}$$

$$\omega_k = \omega_1 + \left(k - \frac{1}{2}\right)\Delta\omega \qquad k = 1,2,\dots,N \quad \text{و} \quad \Delta\omega = (\omega_2 - \omega_1)/N \tag{30}$$

For the purposes of this research, the grade 3 of the track irregularities in the horizontal and the vertical directions are reproduced. The results are presented in Figs. 7(a) and 7(b). These are used as the initial conditions to solve the system motion equations for the tank car at curve. The vertical track irregularities are applied as the displacements to the bottom of the primary suspension system.

3.1.2 The track geometrical specifications

For the purposes of this research part of the track including a tangent track, the transition curve and the main curve are considered. It is also assumed that in wheel maneuvering from the transition curve to the main curve the Kalker’s coefficients remain constant and do not have much of influence on the input excitations. The proposed model for the wheelset is useful for curves with radiuses larger than 700 m. In this research a curve with a radius of 700 m is used.

4. The active suspension system

The aim is to control the destructive effects of the harmonic sloshing in the tank cars. This can be achieved by designing a proper control mechanism for the suspension system. Hence, converting the available passive suspension into an active controlled one. It can be done by adding controllable hydraulic jacks to the rest of the suspension system components. These jacks need to be mounted between the bogie and the car body. Each bogie needs to be equipped with two jacks.

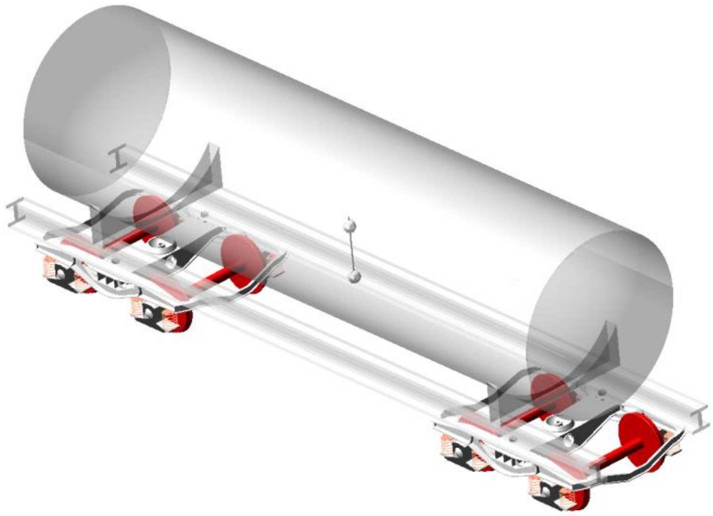

Fig. 8 Schematic of a tank car on two bogies candid for mounting four controlled hydraulic jacks

Consequently each car will have four hydraulic jacks. The proposed hydraulic jacks are used in order to provide the forces required for the active control of the car body. A schematic for the rail vehicle on two bogies is presented in Fig. 8.

4.1 Designing the feedback controller

The most important measures for the performance of the rail vehicle suspension systems are the ability to provide dynamic stability for the vehicle and the reduction in the acceleration that transmits to the car body. The input to this system is the wheel displacement that causes the relative displacement between the sprung and the un-sprung masses. In a tank car such excitations influence the components of the vehicle as well as the liquid inside the tank. This causes the oscillatory motion of the liquid that can last for a considerable length of time. The design procedure of a controller that can minimize the unwanted oscillations starts by considering 44 state variables. These include the displacement and the velocities of all the degrees of freedom already introduced in the system motion equations. The state variables are the displacement and the velocity associated to the degrees of freedom of the components of the car body, the bogies and the pendulum. Consequently, the system state matrix is defined according to the following equations

$$x = [x_1\ x_2\ x_3\ \dots\ x_{43}\ x_{44}] \tag{31}$$

Therefore, the modeling continues with a linear time invariant system in the following from

$$\dot{x} = Ax + Bu + Gw \tag{32}$$

In this equation A, B and G are the matrices corresponding to the input and the disturbances to the system, respectively. The state variable feedback regulator is defined as

$$u = -Kx \tag{33}$$

Where K is the feedback gain matrix. The optimized controller needs to minimize the cost function in Eq. (34).

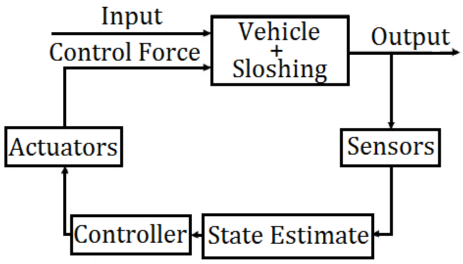

Fig. 9 Flow diagram of the solution method

$$J = \int_0^\infty (x^T Q x + u^T R u) dt \tag{34}$$

Where =[*f*], *R* and Q are the positive definite weighing matrices. The theory of the optimized linear control recommends coefficient *K* as in Eq. (35) for LTI form of solution for Eq. (34)

$$K = R^{-1} B^T P \tag{35}$$

Where *P* comes from the Algebraic solution to the Ricatti formula

$$A^T P + PA - PBR^{-1} B^T P + Q = 0 \tag{36}$$

By substituting *K* in Eq. (32), the controlled state variables take the following form

$$\dot{x} = (A - BK)x + Gw \tag{37}$$

5. Solving the system motion equations

After designing the feedback based on the intrinsic properties of the system, combination of the system dynamic equations and the liquid sloshing are solved under the initial conditions that includes the curved track with irregularities (Fig. 9).

During each time step the state variables for all of the degrees of freedom are evaluated and multiplied by the designed control coefficient. The obtained values as control forces are entered to system by actuators. These coefficients are designed in such way that the actuating forces cause reduction in the ultimate values of the state variables. Therefore, the total displacement of the system reduces and consequently the whole system stability improves.

6. The results and discussions

6.1 The pendulum angular motion

When studying the outcomes of the modeling, the pendulum angular motion represents the liquid motion in the lateral direction. The variations in the pendulum angular motion for a Parsi tank car traveling over a curved track of 700 m in length at a constant speed of 40 km/h is presented in Fig. 10. At this section of the track the length of the transition curve is 100 m and the length of the main curve is 600 m. The track cant angle of inclination at the main curve is 5o. The

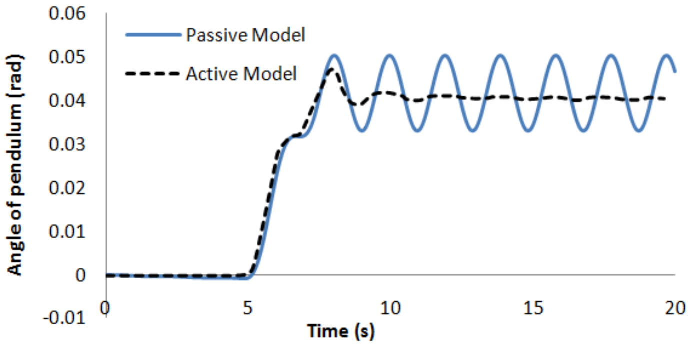

Fig. 10 The angular motion of the pendulum when negotiating a curve

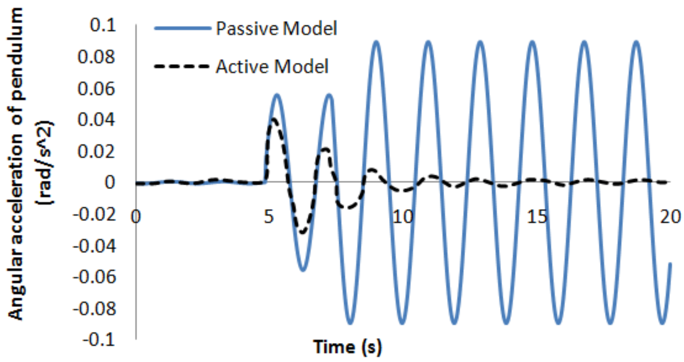

Fig. 11 The pendulum angular acceleration

vehicles enter the transition curve at time *t*=5 sec and the main curve at *t*=7 sec. The results are for two cars one with passive suspension and the other one equipped with active suspension system. It is observed that in both cases as the vehicles enter the curve centrifugal forces push the pendulums to deviate from their resting positions.

In the continuation of the motion, when the vehicles enter the main curve at *t*=7 sec the pendulums start oscillatory motions. The onset of the oscillations can be attributed to the excitations generated by the changes in the radius of curvature of the track as the vehicles exit the transition curve and enter the main curve. In the passive mode, the pendulum starts oscillating around the initial angle of deviation. In the active mode the oscillatory motion of the pendulum dies out. Such damping effect can also impinge on other degrees of freedom. Another decisive factor is the acceleration of the car body. This is also calculated for both vehicles and the results are presented in Fig. 11. The dynamic sloshing index that is a critical parameter in the design of the tank shells can be calculated by using the car body acceleration.

According to the results that are presented in Fig. 11, as the vehicles enter the transition curves at *t*=5 sec the car body acceleration starts building up. At this section of the track it reaches to a maximum of 0.06 rad/s2 for inactive suspension and to a maximum of 0.04 rad/s2 for the vehicle with an active suspension system. In the main section of the curve, in case of the vehicle with the passive suspension, the pendulum acceleration oscillations with constant amplitude of approximately 0.09 rad/s2. In case of the vehicle with active suspension the amplitude of acceleration attenuates and quickly dies out.

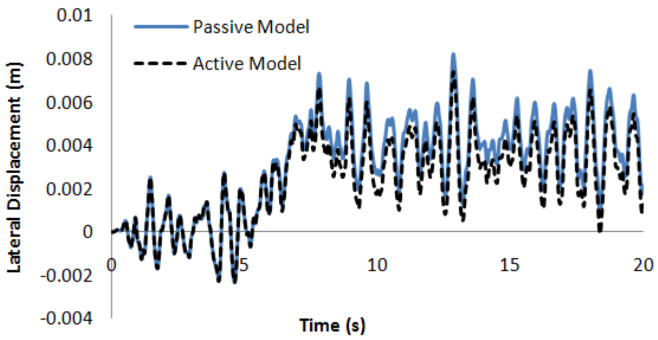

Fig. 12 The lateral displacement of the tank car's 1st wheelset

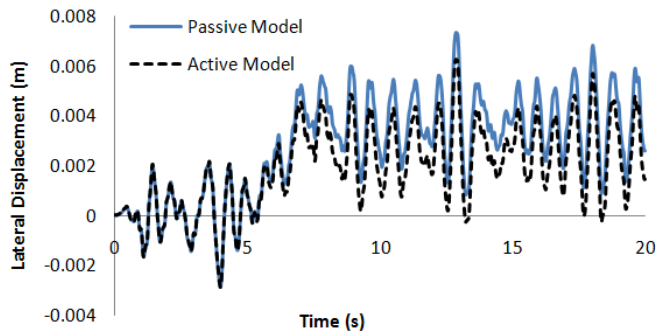

Fig. 13 The lateral displacement of the tank car's 2nd wheelset

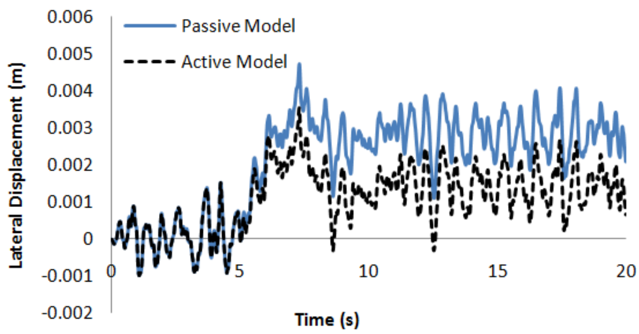

Fig. 14 The lateral displacement of the tank car's 3rd wheelset

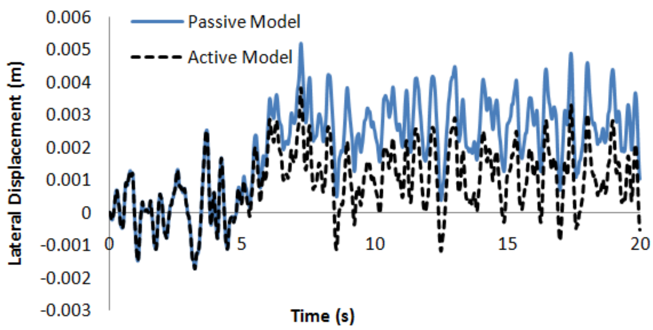

Fig. 15 The lateral displacement of the tank car's 4th wheelset

Table 3 Peak values for the wheelsets lateral displacements in the passive and active models

Wheel No	Passive Model (mm)	Active Model (mm)	Reduction Percentage (%)
1	0.0082	0.00741	9.75
2	0.00736	0.00624	15.2
3	0.00472	0.00355	24.7
4	0.00518	0.00383	26.0

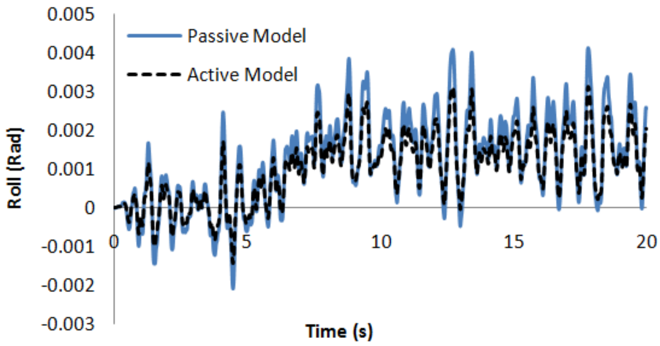

Fig. 16 The roll angle in the tank car 1st wheelset

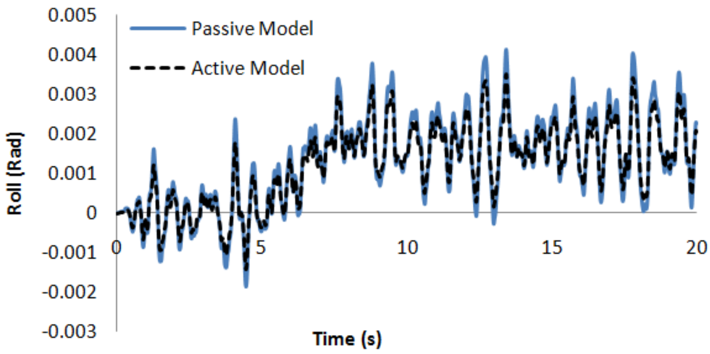

Fig. 17 The roll angle in the tank car 2nd wheelset

6.2 The lateral motion of the vehicle components

6.2.1 The wheelset

Study of the lateral motion of the wheelsets is important because of fatigue investigation in axles. The lateral motion of the wheelsets 1-4 (from front to rear) that were represented by 2 degrees of freedom are also calculated. These are presented in Figs. 12-15.

From these results that also correspond to the Parsi tank car particulates, it is clear that the track irregularities have negligible effects in the wheelset displacements in tangent tracks and in parts of the transition curve in either passive or active models. However, such effects are clearly present at the main curve. Also, the control system is more effective in case of the rear wheels. The peak values in the horizontal displacement of the wheelsets in the passive and active models are calculated and presented in Table 3. Clearly the maximum displacements in the front wheelsets are higher than the rear wheelsets. This happens while the control system shows better performance on

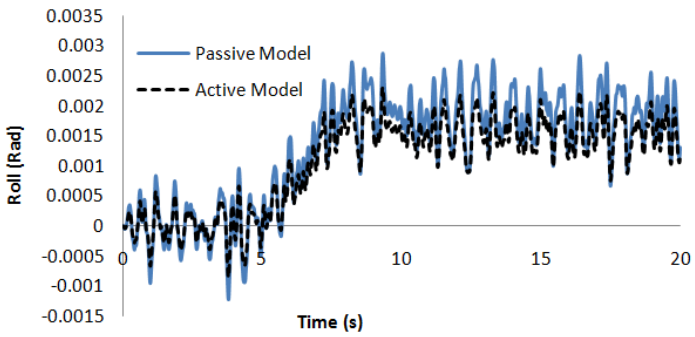

Fig. 18 The roll angle in the tank car 3rd wheelset

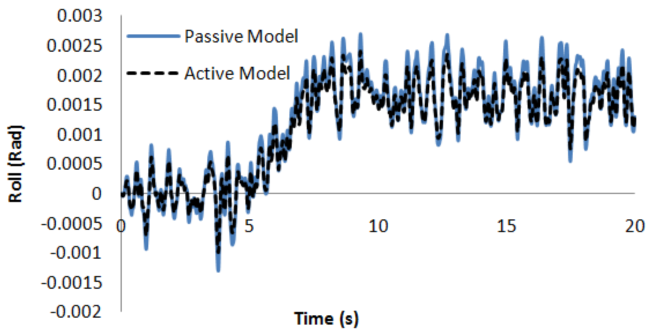

Fig. 19 The roll angle in the tank car 4th wheelset

Table 4 Comparisons of the wheelset roll angles for the vehicles with and without the active suspension system

Wheelset No	The passive suspension model (Rad)	The active suspension model (Rad)	Reduction in percentage (%)
1	0.00414	0.00314	24.15
2	0.00413	0.00351	15.00
3	0.00287	0.00231	19.51
4	0.0027	0.00241	10.00

the rear wheelsets.

The calculated wheelset roll angles are also presented in Figs. 16-19. Also, in these cases the presence of the active suspension system causes reduction in the amplitude of the roll angle. The roll angle is calculated as the difference between the absolute roll angle of the wheelset and the track cant inclination angle.

The peak values for the wheelset roll angles for the vehicle with the passive suspension system and the vehicle with the active suspension system are presented in Table 4.

6.3 The bogie

Bogies are major players in the configuration of the rail vehicles. Bogies take the vehicle load and facilitate the motion. Foremost efforts in maintaining the rail vehicle and its bogies point

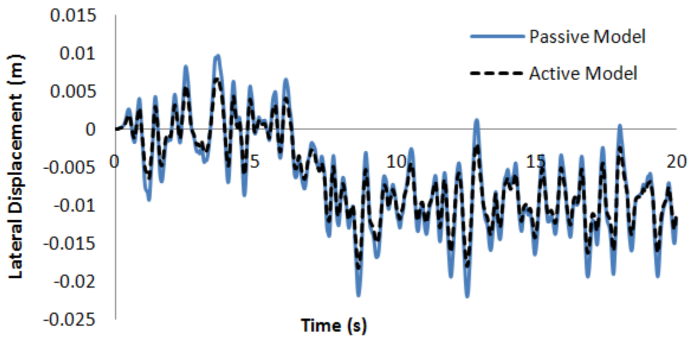

Fig. 20 The lateral displacement of the front bogie at curve

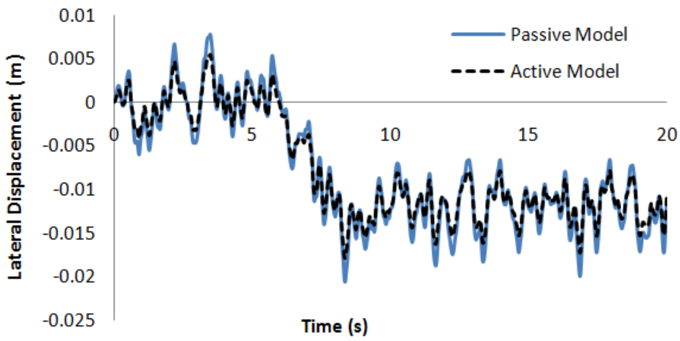

Fig. 21 The lateral displacement of the rear bogie at curve

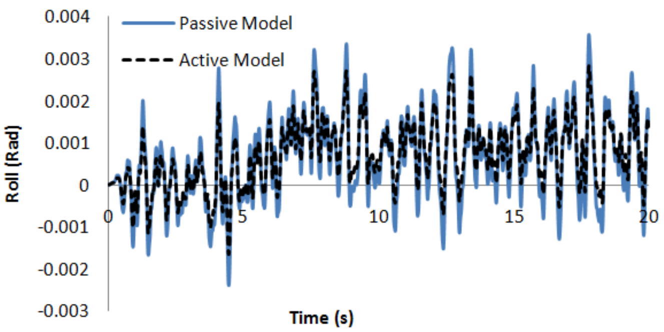

Fig. 22 The roll angle at the front bogie of the Parsi tank car at curve

toward preventing the bogies frame deformation that mainly happens at curves. In case of the sample run with Parsi tank cars the lateral displacements of the bogies are calculated and presented in Figs. 20 and 21. In Fig. 20 the maximum horizontal displacement for the front bogie is presented with and without the active suspension system. They mount up to 0.0183 m with the controller and 0.022 m without the controller. It shows a reduction of 16.8% in the bogie displacement when the active suspension system is used. In case of the rear bogie these values mount up to 0.01797 and 0.0206 m for the active and the passive cases, respectively. That is a reduction of 12.7% in the lateral displacement of the rear bogie at the presence of the active suspension system.

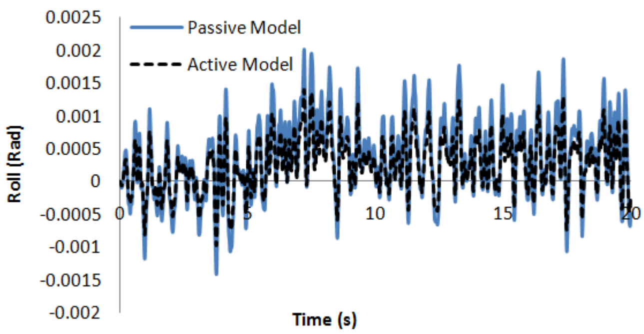

Fig. 23 The roll angle at the rear bogie of the Parsi tank car at curve

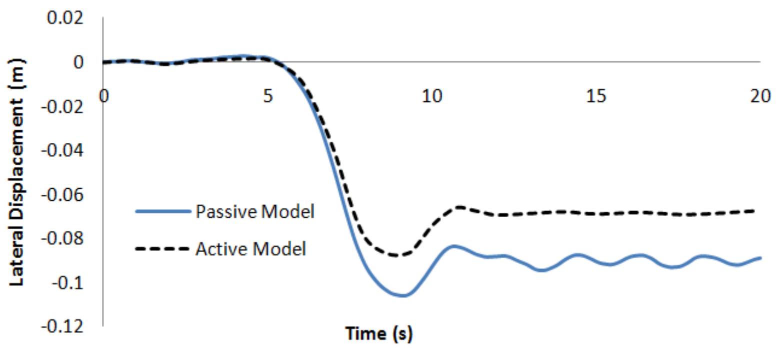

Fig. 24 The car body lateral displacement at curve

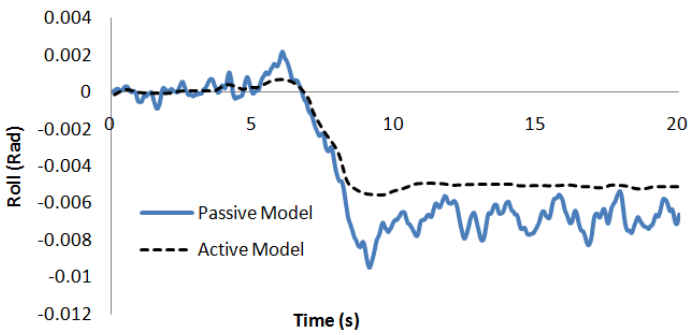

Fig. 25 The car body roll angle at curve

Since sloshing clearly affects the roll motion as well as the lateral displacement the roll angle for the bogies are also calculated and presented in Figs. 22 and 23. These are the differences between the absolute roll angle and the cant inclination angle at curve. Reduction in the maximum roll angles in the rear and the front bogies at the presence of the active suspension system are 23% and 26%, respectively.

6.4 The car body

Exciting the liquid at curves initiates its oscillations and this in turn starts the liquid load and

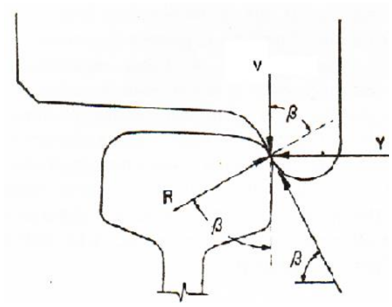

Fig. 26 Contact forces at the wheel/rail contact at the instant of derailment

the tank interactions. With the sample run of a Parsi tank car, the lateral displacement and the roll angle of the car body are presented in Fig. 24 and Fig. 25, respectively. In the tank car with the passive suspension system the influence of the liquid oscillations on the car body at the main curve is obvious. This is while in the case of the tank car with the active suspension system during traversing the curve the car body oscillations die out and the amplitude of vibrations reduces, subsequently.

In the case of the vehicle with passive suspension system the roll angle is completely under the influence of the liquid movements at the main section of the curve. The effect of the liquid sloshing on the tank shell is obvious. By using the active suspension system such oscillations are minimized while the vehicle negotiates the main curve. Reduction in the maximum car body roll angle and lateral displacement at the presence of the active suspension system are 45% and 21%, respectively.

7. The Nadal's derailment index

Of the many scenarios for the rail vehicle derailment one is the climbing of the wheel flange on the rail. This can be very hazardous and end up to unrecoverable consequences. The studies on the rail vehicle derailment started in 1908 when Nadal assumed that at the onset of the wheel climbing onto the rail the wheel and the rail contact in two points. The 1st point is on the rolling surface of the wheel and acts as the instantaneous centre of rotation of the wheel on the rail. The 2nd contact point is on the wheel flange that plays the main role on the wheel climbing the rail. With such an assumption the balance of the forces acting on the wheel/rail contact area results in Eq. (38) that is known as the Nadal equation. A schematic of the contact points and the acting forces is presented in Fig. 26.

$$\frac{L}{V} = \frac{\tan\beta - \mu}{1 + \mu \tan\beta} \tag{38}$$

Where β is the flange (or the wheel contact) angle, μ is the friction coefficient at the wheel/rail contact surface.

Nadal proposed that if the wheel flange contact angle is 65o the maximum *L/V* ratio (or the derailment index) is equal to 0.79. This was subsequently approximated to 0.8 and was introduced as the wheel derailment index and has been widely in use by the industrial centers (UIC 1999).

Preventing derailment turns to be a major task for safeguarding railway transportation systems.

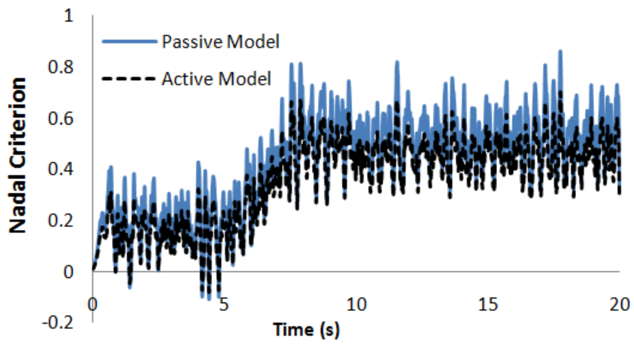

Fig. 27 The Nadal index for the front left wheel of the front bogie for the tank car negotiating a curve

Due to its importance, it is worth working out the influence of the active suspension system on the derailment index and its dynamic stability.

Therefore, with the Parsi tank car model model available while the vehicle traverses the curved track the Nadal derailment index is also calculated. The calculations are for the two cases of the tank car with and without the active suspension system. The results are for the front left wheel of front bogie in the tank car and are presented in Fig. 27. It is noticeable that by the tank car entering the curve the Nadal index and subsequently the risk for the derailment increase. In the case of the vehicle with passive suspension system this index reaches to values higher than 0.8. By installing the active suspension system the maximum value for the Nadal index shows 0.095 reduction.

The noticeable point is that such active suspension system is also effective in the longitudinal direction. It can assist the fleet longitudinal stability during the acceleration and the braking procedures. This can be a subject for future studies.

8. Conclusions

In this paper, the dynamic analysis of partially filled tank car travelling on curved track is investigated. On the whole, 22 degrees of freedom were considered, 21 of them have been allocated to tank car and one of them was related to pendulum equalizing fluid sloshing in lateral direction (around x axis).

Using LQR method and active suspension system, the displacement of wheels, bogies and tank car are decreased. This causes reduction in the side effects such as the fatigue of bogies and axles. Consequently, the cost of maintenance of the vehicles reduces.

1. It is shown that the use of active control decreases the lateral displacement of the 1st to the 4th wheels of the wagon to the equivalents of 9.75%, 15.2%, 24.7%, and 26%, respectively. These are calcultaed in comparison with the cases with passive suspension.

2. The 1st to the 4th wheelsets rolls have been mitigated to 24.15%, 15%, 19.51% and 10% respectively.

3. The reduction percentages of lateral and roll displacement of bogies are remarkable too.

4. The research shows 16.8% and 12.7% reduction in lateral displacement and 23% and 26% reduction in roll displacement.

5. The use of LQR has significantly reduced the maximum car body roll angle and the lateral displacements to 45% and 21%, respectively.

6. At the presence of the active suspension system, the angular acceleration and the displacement of the pendulum as effective parameters on fluid solid interaction force attenuate rapidly. They turn to be stable while in passive one. The fluid oscillates for a period of time.

7. Considering the increasing importance of tank cars, attention on stability and improving the track safety find prime importance. Nadal's derailment index effectively presents the condition of rolling stock safety and stability. By using the proposed suspension system, this index can be lowered to about 0.1. Therefore the risk of derailment decreases, especially during traveling on curved tracks.

Nomenclature

a	half of track gauge
b_1	half of primary yaw spring arm and primary yaw damping arm
b_1	half of primary vertical spring arm and primary vertical damping arm
b_2	half of secondary longitudinal spring arm and secondary vertical spring arm
b_3	half of secondary longitudinal damping arm and secondary vertical damping arm
C_{px}	Damping coefficient of primary suspension in longitudinal direction
C_{py}	Damping coefficient of primary suspension in lateral direction
C_{pz}	Damping coefficient of primary suspension in vertical direction
C_{sx}	Damping coefficient of secondary suspension in longitudinal direction
C_{sy}	Damping coefficient of secondary suspension in lateral direction
C_{sz}	Damping coefficient of secondary suspension in vertical direction
f_{11}	lateral creep force coefficient
f_{12}	lateral/spin creep force coefficient
f_{22}	spin creep force coefficient
f_{33}	longitudinal creep force coefficient
F_{ki}	Force related to designed control system
F_{kxij}	linear creep force acting in longitudinal direction on left and right wheels in front and rear wheelsets
F_{kyij}	linear creep force acting in lateral direction on left and right wheels in front and rear wheelsets
F_{szti}	suspension force acting in vertical direction on front and rear truck frames
F_{syc}	suspension force acting in lateral direction on half car body
F_{syij}	suspension force acting in lateral direction on front and rear wheelsets
F_{syti}	suspension force acting in lateral direction on front and rear truck frames
F_{szc}	suspension force acting in vertical direction on car body
h	height of external weight above center of gravity of wheelset
h_C	vertical distance from wheelset center of gravity to car body
h_T	vertical distance from wheelset center of gravity to secondary suspension
I_{cx}	equivalent roll moment of inertia of car body and fixed fluid mass
I_{cy}	equivalent pitch moment of inertia of car body and fixed fluid mass
I_{cz}	equivalent yaw moment of inertia of car body and fixed fluid mass

I_{tx}	roll moment of inertia of truck frame
I_{tz}	yaw moment of inertia of truck frame
I_{wx}	roll moment of inertia of wheelset
I_{wy}	spin moment of inertia of wheelset
I_{wz}	yaw moment of inertia of wheelset
i=1, 2	indices denoting front and rear of truck, respectively
j =1, 2	indices denoting front and rear wheelsets, respectively
$k = L,R$ or 1,2	indices denoting left and right wheels and sides of bogie, respectively
K_{px}	longitudinal stiffness of primary suspension
K_{py}	lateral stiffness of primary suspension
K_{pz}	vertical stiffness of primary suspension
K_{sx}	longitudinal stiffness of secondary suspension
K_{sy}	lateral stiffness of secondary suspension
K_{sz}	vertical stiffness of secondary suspension
L_1	half of primary lateral spring arm
L_2	half of primary lateral damping arm
L_c	longitudinal distance from wheelset center of gravity to car body
m_c	car body and fixed fluid mass
m_t	truck frame mass
m_w	wheelset mass
M_{sxc}	suspension moment acting in longitudinal direction on car body
M_{sxti}	suspension moment acting in longitudinal direction on front and rear truck frames
M_{syc}	suspension moment acting in lateral direction on car body
M_{szc}	suspension moment acting in vertical direction on car body
M_{szij}	suspension moment acting in vertical direction on front and rear wheelsets
M_{szti}	suspension moment acting in vertical direction on front and rear truck frames
M_{kxij}	linear creep moment acting in longitudinal direction on left and right wheels in front and rear wheelsets
M_{kzij}	linear creep moment acting in vertical direction on left and right wheels in front and rear wheelsets computed using Kalker’s linear theory
N	normal force acting on wheelset in equilibrium state
N_{Lyij}	normal force acting in lateral direction on left wheel in front and rear wheelsets
N_{Lzij}	normal force acting in vertical direction on left wheel in front and rear wheelsets
N_{Ryij}	normal force acting in lateral direction on right wheel in front and rear wheelsets
N_{Rzij}	normal force acting in vertical direction on right wheel in front and rear wheelsets
r_L	rolling radius of left wheel
r_R	rolling radius of right wheel
r_0	nominal rolling radius of wheelset
R	radius of curvature of track
R_{Lxij}	x component of position vector on left wheel in front and rear wheelsets
R_{Lyij}	y component of position vector on left wheel in front and rear wheelsets

R_{Rxij}	x component of position vector on right wheel in front and rear wheelsets
R_{Ryij}	y component of position vector on right wheel in front and rear wheelsets
t	time
V	forward speed of truck
W	axle load
W_{ext}	external load
x, y, z	longitudinal, lateral and vertical coordinates, respectively
y_c	lateral displacement of car body
y_{ti}	lateral displacement of front and rear truck frames
y_{wij}	lateral displacement of front and rear wheelsets
z_c	vertical displacement of car body
z_{ti}	vertical displacement of front and rear truck frames
δ_L	contact angle of left wheel
δ_R	contact angle of right wheel
λ	wheel conicity
θ_c	pitch angle of car body
ϕ_c	roll angle of car body
ϕ_p	roll angle of pendulum
ϕ_{se}	superelevation angle of curved track
ϕ_{ti}	roll angle of front and rear truck frames
ψ_c	yaw angle of car body
ψ_{ti}	yaw angle of front and rear truck frames
ψ_{wij}	yaw angle of front and rear wheelsets
l_p	pendulum beam length
m_p	pendulum mass
I_p	pendulum moment of inertia

m_w	Wheelset mass	1300 kg	m_t	Bogie frame mass	2200 kg
r_0	Wheel radius	0.42 m	a	Half of track gauge	0.7175 m
λ	Wheel conicity	0:05	d	Flange clearance	0.00923 m
f_{11}	Lateral creep force coefficient	2.212e6 N	f_{12}	Lateral/spin creep force coefficient	3120 N m^2
f_{22}	Spin creep force coefficient	16 N	f_{33}	Longitudinal creep force coefficient	2.563e6 N
μ	Coefficient of friction	0.2	m_c	Car body mass	3.1e4 kg
K_{px}	Longitudinal stiffness of primary suspension	1.4e6 N/m	K_{py}	Lateral stiffness of primary suspension	1.4e6 N/m
K_{pz}	Vertical stiffness of primary suspension	1e6 N/m	C_{pz}	Vertical damping of primary suspension	526737 Ns/m
K_{sx}	Longitudinal stiffness of side bearings	1e5 N/m	K_{sy}	Lateral stiffness of side bearings	1e5 N/m
K_{sz}	Vertical stiffness of side bearings	5.7e5 N/m	C_{sx}	Longitudinal damping of side bearings	0 N.s/m

C_{sy}	Lateral damping of side bearings	0 N.s/m	C_{sz}	Vertical damping of ide bearings	1000 N.s/m
b_1	Half of primary longitudinal and vertical spring / damping arm	1.0 m	b_2	Half of secondary longitudinal and vertical spring arm	1.18 m
b_3	Half of side bearings longitudinal and vertical damping arm	1.4 m	N	Normal force acting on wheelset in equilibrium state	N
L_2	Half of primary lateral damping arm	1.5 m	L_1	Half of primary lateral spring arm	1.28 m
L_c	Longitudinal distance from wheelset center of gravity to car body	4.2 m	h_T	Vertical distance from wheelset center of gravity to side bearings	0.47 m
I_{wx}	Roll moment of inertia of wheelset	688 kg.m^2	I_{wy}	Spin moment of inertia of wheelset	100 kg.m^2
I_{wz}	Yaw moment of inertia of wheelset	688 kg.m^2	I_{tx}	Roll moment of inertia of bogie frame	1995 kg.m^2
I_{tz}	Yaw moment of inertia of bogie frame	2850 kg.m^2	I_{cx}	roll moment of inertia of car body	3.7e4 kg m^2
I_{cz}	yaw moment of inertia of car body	2.98e4 kg m^2	I_{yy}	Length of pendulum for 50% partially filled tank car	0.95 m
L	Pendulum mass for 50% partially filled tank car	18304.6 kg			

References

Abramson, H.N. (1966), “The Dynamic Behavior of Liquids in Moving Containers”, NASA-SP-106..

Au, F.T.K. (2002), “Impact study of cable-stayed railway bridges with random rail irregularities”, *Eng. Struct.*, **24**, 529-541.

Aliabadi, S., Johnson, A. and Abedi, J. (2003), “Comparison of finite element and pendulum models for simulation of sloshing”, *Comput. Fluid.*, **32**, 535-545.

Cakir, T. and Livaoglu, R. (2013), “Experimental analysis on FEM definition of backfill-rectangular tank-fluid system”, *Geomech. Eng.*, **5**(2), 165-185.

Cheng, Y., Lee, S. and Chen, H. (2009), “Modeling and nonlinear hunting stability analysis of high-speed railway vehicle moving on curved tracks”, *J. Sound Vib.*, **324**, 139-160

Evans, J.R. and Rogers, P.J. (1998), “Validation of dynamic simulations of rail vehicles with friction damped Y25 bogies”, *Veh. Syst. Dyn.*, **29**(1), 219-233.

Frýba, L. (1996), “Dynamics of Railways Bridges”, Thomas Telford House, Czech Republic.

GM/GN2688 (2010), “Guidance on the Structural Design of Rail Freight Wagons including Rail Tank Wagons”, Rail Industry Guidance Note for GM/RT2100, Issue Four.

USA, DOT/FRA/ORD-06/16.

Lee, S. and Cheng, Y. (2005), “Hunting stability analysis of higher-speed railway vehicle trucks on tangent tracks”, *J. Sound Vib.*, **282**, 881-898.

Lee, S. and Cheng, Y. (2006), “Influences of the vertical and the roll motions of frames on the hunting

stability of trucks moving on curved tracks", *J. Sound Vib.*, **294**, 441-453.
Locovei, C., Radula, A., Nicoara, M. and Cucuruz, L.A. (2010), "Analysis of fatigue fracture of tank wagon railway axles", *Proceedings of the 3rd WSEAS Int. Conference on Finite diffrences - Finite elements - Finite Volume - Boundary Elements,* Romania.
Molatefi, H., Hecht, M. and Kadivar, M.H. (2006), "Critical speed and limit cycles in the empty Y25-freight wagon", *Proceedings of the Institution of Mechanical Engineers, Part F: Journal of Rail and Rapid Transit*, **220**(4), 347-359.
Nadal, M.J. (1908), "Locomotive a vapeur,Collection Encyclopedie scientific, Biblioteque de Mechanique Appliquee et Genie", 186, Paris.
Ormeño, M., Larkin, T. and Chouw, N. (2012), "Influence of uplift on liquid storage tanks during earthquakes", *Coupl. Syst. Mech*., **1**(4), 311-324.
Prabhakaran, A., Trent, R. and Sharma, V. (2005), "Impact Performance of Draft Gears in 263,000 Pound Gross Rail Load and 286,000 Pound Gross Rail Load Tank Car Service", Federal Railroad Administration.
Sumner, I.E. (1965), "Experimentally Determined Pendulum Analogy of Liquid Sloshing in Spherical and Oblate-Spheroidal Tanks", NASA-TN-2637.
Tan, X. and Rogers, R.J. (1995), "Equivalent Viscous damping models of coulomb friction in multi degree freedom vibration systems", *J. Sound Vib.*. **185**(1), 33-50.
UIC (1999) Leaflet 518 (draft), "Test and approval of railway vehicles from the points of view of dynamic behavior, safety, track fatigue and ride quality", International Union of Railways.
Vera, C., Paulin, J., Suárez, B. and Gutiérrez, M. (2005), "Simulation of freight trains equipped with partially filled tank containers and related resonance phenomenon", *Proceedings of the Institution of Mechanical Engineers, Part F: Journal of Rail and Rapid Transit,* **219**(4), 245-259.
Wang, T.L. (1992), "Impact in a railway truss bridge", *Comput. Struct. J.*, **49**(6), 1045-1054.
Wiriyachai, A., Chu, K.H. and Garg, V.K. (1982), "Bridge impact due to wheel and track irregularities", *J. Eng. Mech. Div.*, ASCE, **108**(4), 648-666.
Younesian, D., Abedi, M. and Hazrati Ashtiani, I. (2010), "Dynamic analysis of a partially filled tanker train travelling on a curved track", *Int. J. Heavy Veh. Syst.*, **17**(3-4), 331-358.
Zeng, J. and Wu, P. (2004), "Stability analysis of high speed railway vehicles", *JSME Int. J., Series C: Mech. Syst., Mach. Elem. Manufact.*, **47**(2), 464-470.
Zhou, R., Zolotas, A. and Goodall, R. (2011), "Integrated tilt with active lateral secondary suspension control for high speed railway vehicles", *Mechatronics*, **21**(6), 1108-1122.